

**Observation of linear to planar structural transition in sulfur-doped gold clusters: Au<sub>x</sub>S (x = 2–5)**

Hui Wen, Yi-Rong Liu, Teng Huang, Kang-Ming Xu, Wei-Jun Zhang, Wei Huang, and Lai-Sheng Wang

Citation: *The Journal of Chemical Physics* **138**, 174303 (2013); doi: 10.1063/1.4802477

View online: <http://dx.doi.org/10.1063/1.4802477>

View Table of Contents: <http://scitation.aip.org/content/aip/journal/jcp/138/17?ver=pdfcov>

Published by the [AIP Publishing](#)

---

**Articles you may be interested in**

Photoelectron spectroscopy of boron-gold alloy clusters and boron boronyl clusters: B<sub>3</sub>Au<sub>n</sub> and B<sub>3</sub>(BO)<sub>n</sub> (n = 1, 2)

*J. Chem. Phys.* **139**, 044308 (2013); 10.1063/1.4816010

On the structures and bonding in boron-gold alloy clusters: B<sub>6</sub>Au<sub>n</sub> and B<sub>6</sub>Au<sub>n</sub> (n = 13)

*J. Chem. Phys.* **138**, 084306 (2013); 10.1063/1.4792501

A photoelectron spectroscopy and density functional study of di-tantalum boride clusters: Ta<sub>2</sub>B<sub>x</sub> (x = 2–5)

*J. Chem. Phys.* **138**, 034308 (2013); 10.1063/1.4776769

Influence of the cluster dimensionality on the binding behavior of CO and O<sub>2</sub> on Au<sub>13</sub>

*J. Chem. Phys.* **136**, 024312 (2012); 10.1063/1.3676247

Structure evolution of gold cluster anions between the planar and cage structures by isoelectronic substitution: Au<sub>n</sub> (n = 13–15) and MAu<sub>n</sub> (n = 12–14; M = Ag, Cu)

*J. Chem. Phys.* **134**, 054306 (2011); 10.1063/1.3533443

---



Re-register for Table of Content Alerts

Create a profile.



Sign up today!



# Observation of linear to planar structural transition in sulfur-doped gold clusters: $\text{Au}_x\text{S}^-$ ( $x = 2-5$ )

Hui Wen,<sup>1</sup> Yi-Rong Liu,<sup>1</sup> Teng Huang,<sup>1</sup> Kang-Ming Xu,<sup>1</sup> Wei-Jun Zhang,<sup>1,2</sup> Wei Huang,<sup>1,2,a)</sup> and Lai-Sheng Wang<sup>3,a)</sup>

<sup>1</sup>Laboratory of Atmospheric Physico-Chemistry, Anhui Institute of Optics and Fine Mechanics, Chinese Academy of Sciences, Hefei, Anhui 230031, China

<sup>2</sup>School of Environmental Science and Optoelectronic Technology, University of Science and Technology of China, Hefei, Anhui 230026, China

<sup>3</sup>Department of Chemistry, Brown University, Providence, Rhode Island 02912, USA

(Received 17 February 2013; accepted 8 April 2013; published online 2 May 2013)

We report a joint experimental and theoretical study on the structures of a series of gold clusters doped with a sulfur atom,  $\text{Au}_x\text{S}^-$  ( $x = 2-5$ ). Well-resolved photoelectron spectra are obtained and compared with theoretical results calculated using several density functional methods to elucidate the structures and bonding of  $\text{Au}_x\text{S}^-$  ( $x = 2-5$ ).  $\text{Au}_2\text{S}^-$  is found to have an asymmetric linear global minimum structure with  $C_{\infty v}$  symmetry, while the most stable structure of neutral  $\text{Au}_2\text{S}$  is bent with  $C_{2v}$  symmetry, reminiscent of  $\text{H}_2\text{S}$ .  $\text{Au}_3\text{S}^-$  is found to have an asymmetric bent structure with an Au-S-Au connectivity. Two isomers are observed experimentally to co-exist for  $\text{Au}_4\text{S}^-$ : a symmetric bent 1D structure ( $C_{2v}$ ) and a 2D planar low-lying isomer ( $C_s$ ). The global minimum of  $\text{Au}_5\text{S}^-$  is found to be a highly stable planar triangular structure ( $C_{2v}$ ). Thus, a 1D-to-2D structural transition is observed in the  $\text{Au}_x\text{S}^-$  clusters as a function of  $x$  at  $x = 4$ . Molecular orbital analyses are carried out to obtain insight into the nature of the chemical bonding in the S-doped gold clusters. Strong covalent bonding between S and Au is found to be responsible for the 1D structures of  $\text{Au}_x\text{S}^-$  ( $x = 2-4$ ), whereas delocalized Au-Au interactions favor the 2D planar structure for the larger  $\text{Au}_5\text{S}^-$  cluster. © 2013 AIP Publishing LLC. [<http://dx.doi.org/10.1063/1.4802477>]

## I. INTRODUCTION

Gold exhibits many unique properties among the coinage metals because of the strong relativistic effects.<sup>1,2</sup> Nanoscale gold clusters and particles have attracted much attention since the discovery of unexpected physical and chemical properties that can be exploited for a variety of applications, ranging from catalysis, nanotechnology, nanobiology, and microelectronics, to important luminescent, photosensitive, and optical materials.<sup>3,4</sup> Bare Au clusters ( $\text{Au}_n^-$ ) have been well studied and they show distinctive structures, interesting structural transitions, and size-dependent chemical properties.<sup>5-45</sup> Doping gold clusters with heterogeneous atoms is expected to open up new research opportunities to enhance the stability of gold clusters and modify their physicochemical properties.<sup>46-72</sup> Varying the dopants provides a new route to tailor the properties of nanoclusters, in addition to tuning the cluster size and shape.

The study of sulfur-doped gold clusters ( $\text{Au}_x\text{S}_y$ ) has received much attention, motivated in part by understanding the Au-S interactions, which are important in thiol-passivated gold nanoparticles. Sulfur has also been identified as the most suitable “clipping” atom between molecular devices and gold electrodes.<sup>73-75</sup> There have been a number of experimental<sup>72,76-80</sup> and theoretical<sup>73,74,80-86</sup> investigations on the reactivity of gold clusters with sulfur. Positive and

negative Au-S cluster ions were first examined by Zheng and co-workers using laser ablation time-of-flight mass spectrometry.<sup>79</sup> Lineberger and co-workers reported a high resolution photoelectron spectrum of  $\text{AuS}^-$  at 364 nm for the ground-state transition.<sup>78</sup> Zhai *et al.* studied monogold sulfide clusters ( $\text{AuS}^-$  and  $\text{AuS}_2^-$ ) as the simplest molecular model to elucidate the Au-S chemical bonding in a combined photoelectron spectroscopy (PES) and *ab initio* study.<sup>72</sup> More recently, Ning *et al.* reported a joint PES and theoretical study on a series of Au-SCH<sub>3</sub> complexes as models for the thiolate-gold nanoparticle interactions.<sup>80</sup>

A number of computational studies have focused on the structural and bonding properties of Au-S clusters using different calculation methods, such as *ab initio* and density functional theory (DFT).<sup>73,74,80-86</sup> The  $\text{SAu}_3^+$  and  $\text{S}(\text{AuPH}_3)_3^+$  species were found to closely reproduce the experimental Au-S-Au bond angles of monomeric  $\text{S}(\text{AuPR}_3)_3^+$  ( $\text{PR}_3 = \text{PPh}_3, \text{PPR}_3$ ), when both correlation and relativistic effects were included using pseudopotential *ab initio* calculations by Pyykkö and co-workers.<sup>86</sup> Garzon and co-worker<sup>74</sup> studied the structures of the lowest-lying isomers of  $\text{Au}_n\text{S}$  ( $n = 1-5$ ) and  $\text{Au}_n\text{S}_2$  ( $n = 1-4$ ) using a post Hartree-Fock second-order perturbative Møller-Plesset method (HF/MP2). Zeng and co-workers used *ab initio* methods to investigate the structural evolution of a family of gold-sulfide cluster anions.<sup>81</sup> The atomic and electronic structure of  $\text{Au}_5\text{M}$  ( $\text{M} = \text{Na}, \text{Mg}, \text{Al}, \text{Si}, \text{P}, \text{S}, \text{and Au}$ )<sup>85</sup> and  $\text{M@Au}_6$  ( $\text{M} = \text{Al}, \text{Si}, \text{P}, \text{S}, \text{Cl}, \text{and Ar}$ ) clusters<sup>82</sup> have been investigated using DFT with the scalar relativistic effective core potential. Jiang *et al.*<sup>83</sup> studied the

<sup>a)</sup>Electronic addresses: Huangwei6@ustc.edu.cn and Lai-Sheng\_Wang@brown.edu

structures of several large  $\text{Au}_x\text{S}_y^-$  nanoclusters and found a unique core-in-cage structure. The interaction of a single sulfur atom with cationic gold clusters  $\text{Au}_n^+$  ( $n = 1-8$ ) has also been studied using DFT.<sup>84</sup>

Experimental studies on the  $\text{Au}_x\text{S}$  clusters are relatively scarce<sup>72,76-80</sup> and systematic investigations of anionic sulfur-doped gold clusters ( $\text{Au}_x\text{S}^-$ ) have not been reported. In the current article, we present a PES and theoretical study on the  $\text{Au}_x\text{S}^-$  ( $x = 2-5$ ) clusters. The experimental results are used to compare with theoretical results from a variety of computational methods to probe the structures and chemical bonding in the S-doped gold clusters.  $\text{Au}_2\text{S}^-$  is found to be an asymmetric linear cluster, whereas  $\text{Au}_3\text{S}^-$  is found to be an asymmetric bent species. A symmetric bent structure is found for  $\text{Au}_4\text{S}^-$  as the global minimum with a close-lying planar 2D isomer.  $\text{Au}_5\text{S}^-$  is found to be a triangular planar cluster.

## II. EXPERIMENTAL AND THEORETICAL METHODS

### A. Experimental method

The experiments were carried out using a magnetic-bottle-type PES apparatus equipped with a laser vaporization supersonic cluster source, details of which have been described in Refs. 87 and 88. Briefly, the  $\text{Au}_x\text{S}^-$  ( $x = 2-5$ ) clusters were produced by laser vaporization of an  $\text{Au}_2\text{S}/\text{Au}$  mixed target (containing  $\sim 3\%$  S by atoms) in the presence of a helium carrier gas and analyzed by a time-of-flight mass spectrometer. The desired  $\text{Au}_x\text{S}^-$  ( $x = 2-5$ ) clusters were mass-selected and decelerated before photodetachment by a laser beam in the interaction zone of the magnetic-bottle photoelectron analyzer. The PES experiments were performed at two photon energies: 266 nm (4.661 eV) from an Nd:YAG laser and 193 nm (6.424 eV) from an ArF excimer laser. Effort was made to control cluster temperatures, which has proved essential for obtaining high-quality PES data.<sup>89,90</sup> Photoelectrons were collected at nearly 100% efficiency by the magnetic bottle and analyzed in a 3.5 m long electron flight tube. Time-of flight spectra were collected and converted to kinetic energy ( $E_k$ ) spectra calibrated with the known spectra of  $\text{Au}^-$  and  $\text{Rh}^-$ . The reported electron binding energy spectra were obtained by subtracting the kinetic energy spectra from the respective photon energies. The electron kinetic energy resolution of the PES apparatus was  $\Delta E_k/E_k \approx 2.5\%$ , that is, 25 meV for 1 eV electrons.

### B. Computational methods

We carried out unbiased searches for the global minimum structures of  $\text{Au}_x\text{S}^-$  ( $x = 2-5$ ) using the basin-hopping (BH) method coupled with DFT.<sup>19,20,23,24</sup> To generate the isomer populations in the initial BH search, the gradient-corrected Perdew-Burke-Ernzerhof (PBE) exchange-correlation functional and the double-numerical polarized (DNP) basis set with effective core potentials (ECPs) as implemented in the DMol code were used with a medium level convergence criterion. More than 200 structures were sampled.

The isomers for each cluster were ranked according to their relative energies for further optimization at higher levels.

The 20 lowest-lying isomers in each case were further optimized at the PBE/CRENBL-ECP (hybrid functional/basis set) level of theory based on previous works.<sup>23,24,91</sup> We also examined Becke's three-parameter hybrid exchange functional with Lee, Yang, and Parr (B3LYP), the exchange functional of Tao, Perdew, Staroverov, and Scuseria (TPSS), and the PBE functional together with pseudo-potential coupling Dunning's augmented correlation-consistent aug-cc-pVDZ basis set, polarized and diffuse function 6-31++G\*\* basis set, DZP double zeta with polarization and diffuse LANL2DZdp-ECP basis set, as implemented in the NWCHEM 5.1.1 software package.<sup>92</sup>

Single-point energy calculations were performed with inclusion of the spin-orbit (SO) effect. The simulated photoelectron spectra were obtained by fitting the computed vertical detachment energies (VDEs) with Gaussian functions of 0.04 eV width and the simulated spectra of all candidate isomers at the PBE0/CRENBL-ECP/SO level for the Au atoms and different DFT methods, such as aug-cc-pVTZ basis set, triple polarization 6-311++G(3df,3pd) basis set, the def2-TZVP orbital, and auxiliary basis set for the S atom. The computed binding energies were based on the optimized structures using the NWCHEM 5.1.1 software package.

Harmonic vibrational frequencies were calculated to confirm that the lowest-energy isomers are true minima. All the calculations are spin-restricted for closed-shell molecules and spin-unrestricted for open shell species. Higher level *ab initio* calculations were further carried out to aid in structural assignments, including a scalar relativistic effective core potential and the Stuttgart/Dresden (SDD) basis set and aug-cc-pVDZ geometry optimization at the MP2 and CCSD(T) levels of theory.

## III. EXPERIMENTAL AND COMPUTATIONAL RESULTS

### A. Photoelectron spectroscopy

The photoelectron spectra of  $\text{Au}_x\text{S}^-$  ( $x = 2-5$ ) measured at 266 nm and 193 nm are shown in Fig. 1. The 193 nm spectra (right panel) reveal more detachment transitions, whereas the 266 nm data (left panel) allow the first few PES transitions to be observed with enhanced resolution. Rich spectral features are observed for all  $\text{Au}_x\text{S}^-$  clusters and are labeled with letters. The X band in each case represents the ground state transition, yielding the first adiabatic (ADE) and VDE detachment energies. The 266 nm spectra can give relatively accurate first ADEs, which by definition represent the electron affinities (EAs) for the neutral clusters. Because no vibrational structures are resolved for the X band, the ADE is estimated by drawing a straight line at the leading edge of the ground state transition and then adding the instrumental resolution to the intercept with the binding energy axis. All VDEs were measured from the peak maximum of each band. The measured ADEs and VDEs for all the species are summarized in Table I.

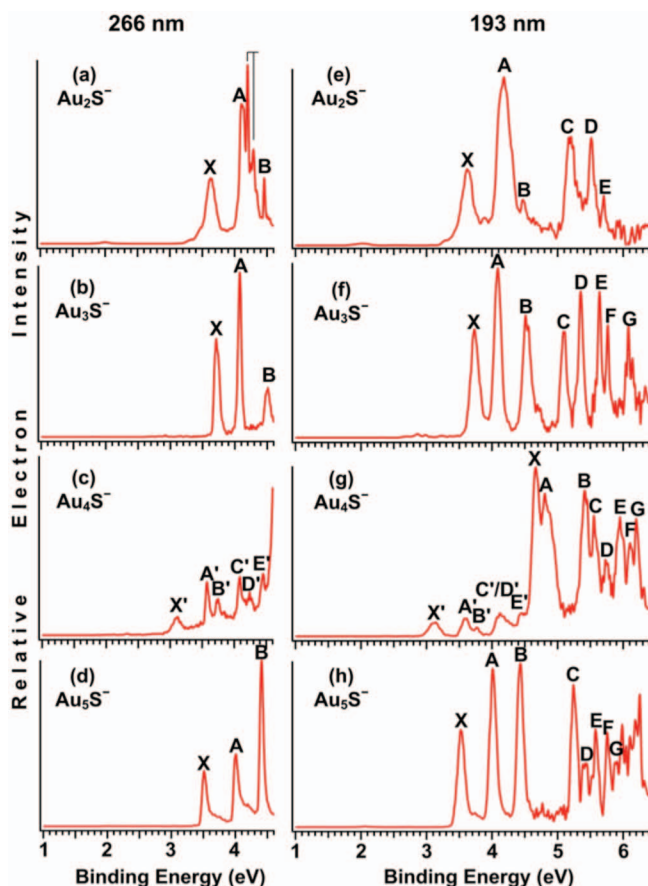


FIG. 1. The photoelectron spectra of  $\text{Au}_x\text{S}^-$  ( $x = 2-5$ ) at 266 nm (4.661 eV) and 193 nm (6.424 eV).

### 1. $\text{Au}_2\text{S}^-$

The 266 nm spectrum of  $\text{Au}_2\text{S}^-$  (Fig. 1(a)) shows at least three detachment transitions (X, A, B). The ADE of band X is estimated to be 3.45 eV, and its VDE is 3.62 eV. Vibrational fine features are resolved for the relatively broadband A (Fig. 1(a)), yielding a vibrational frequency of  $725 \pm 50 \text{ cm}^{-1}$ . The appearance of band A suggests that it may contain several electronic transitions. The separation between bands X and A defines a HOMO-LUMO gap of  $\sim 0.5 \text{ eV}$  for neutral  $\text{Au}_2\text{S}$ . At 193 nm (Fig. 1(e)), three more detachment transitions (C, D, E) are observed in the higher binding energy region.

### 2. $\text{Au}_3\text{S}^-$

The  $\text{Au}_3\text{S}^-$  cluster is closed shell and is expected to yield relatively simple PES spectra. Indeed, eight relatively sharp and well-resolved bands are observed in the 193 nm spectrum of  $\text{Au}_3\text{S}^-$  (Fig. 1(f)). At 266 nm (Fig. 1(b)), three sharp bands (X, A, B) are observed. The first ADE of  $\text{Au}_3\text{S}^-$  or EA of neutral  $\text{Au}_3\text{S}$ , determined from the X band, is 3.64 eV. The sharp X band suggests that there is no significant geometry change between the ground states of  $\text{Au}_3\text{S}^-$  and  $\text{Au}_3\text{S}$ .

TABLE I. Experimental adiabatic (ADE) and vertical (VDE) detachment energies for the main PES bands observed for  $\text{Au}_x\text{S}^-$  ( $x = 2-5$ ) and the computed first ADE and VDE from the global minima. All energies are in eV.

	Observed features	ADE (expt.) <sup>a</sup>	VDE (expt.) <sup>a</sup>	ADE (theo) <sup>b</sup>	VDE (theo) <sup>b</sup>
$\text{Au}_2\text{S}^-$	X	3.45 (4)	3.62 (4)	3.78	3.88
	A		4.20 (4)		
	B		4.47 (5)		
	C		5.18 (4)		
$\text{Au}_3\text{S}^-$	D		5.49 (5)		
	E		5.70 (6)		
	X	3.64 (4)	3.72 (4)	3.52	3.61
	A		4.09 (4)		
	B		4.54 (4)		
	C		5.09 (4)		
	D		5.35 (4)		
$\text{Au}_4\text{S}^-$	E		5.63 (4)		
	F		5.77 (5)		
	G		6.09 (5)		
	X	4.51 (4)	4.66 (4)	4.63	4.70
	A		4.81 (6)		
	B		5.40 (5)		
	C		5.54 (6)		
	D		5.74 (6)		
	E		5.93 (6)		
	X'	2.89 (5)	3.11 (5)	2.93 <sup>c</sup>	3.01 <sup>c</sup>
	A'		3.58 (5)		
B'		3.74 (5)			
C'		4.09 (5)			
D'		4.23 (5)			
E'		4.45 (6)			
$\text{Au}_5\text{S}^-$	X	3.43 (4)	3.52 (4)	3.30	3.39
	A		4.01 (4)		
	B		4.42 (4)		
	C		5.24 (4)		

<sup>a</sup>Numbers in parentheses represent the experimental uncertainties in the last digits.

<sup>b</sup>Calculated first ADE and VDE at the B3LYP/6-311++G(3df,3pd)//B3LYP/6-31++G\*\* level of theory.

<sup>c</sup>Calculated first ADE and VDE for the first low-lying isomer of  $\text{Au}_4\text{S}^-$ .

### 3. $\text{Au}_4\text{S}^-$

The spectra of  $\text{Au}_4\text{S}^-$  are much more complicated and quite different from those of  $\text{Au}_3\text{S}^-$ . At 266 nm (Fig. 1(c)), weak features were observed in the low binding energy side, but there is a strong signal at the high binding energy end, indicating the onset of a much more intense peak. At 193 nm (Fig. 1(g)), we indeed observe at least eight intense peaks beyond 4.5 eV, labeled as X, A–G. The weak features (X', A'–E') at lower binding energies are likely due to a weakly populated low-lying isomer, since their relative intensities depend on the source conditions. These features cannot be eliminated, indicating that the energy of this isomer must be very close to the global minimum. The ADE of the main isomer of  $\text{Au}_4\text{S}^-$  is estimated to be 4.51 eV from the intense X band, whereas the ADE of the low-lying isomer is estimated to be 2.89 eV from the X' feature. The X' and A' bands define a HOMO-LUMO gap of  $\sim 0.5 \text{ eV}$  for the low-lying isomer of  $\text{Au}_4\text{S}$ , suggesting it is a closed-shell neutral species. However, the spectrum of the main isomer of  $\text{Au}_4\text{S}^-$  suggests that

its neutral may have a triplet ground state because there is no HOMO-LUMO gap.

#### 4. $\text{Au}_5\text{S}^-$

The  $\text{Au}_5\text{S}^-$  anion is also closed shell and yields well-resolved PES transitions in the lower binding energy region. At 266 nm (Fig. 1(d)), three sharp and well-resolved peaks (X, A, B) are observed. At 193 nm (Fig. 1(h)), more congested spectral features are observed in the high binding energy range above 5 eV. This is expected because the high binding energy features are probably due to photodetachment from Au 5*d*-derived molecular orbitals. The first ADE of  $\text{Au}_5\text{S}^-$  or EA of neutral  $\text{Au}_5\text{S}$ , determined from the X band, is 3.43 eV. Surprisingly, this is the lowest among all the  $\text{Au}_x\text{S}^-$  species, except that of the low-lying isomer of  $\text{Au}_4\text{S}^-$ . The sharp X band suggests that there is no significant geometry change between the ground states of  $\text{Au}_5\text{S}^-$  and  $\text{Au}_5\text{S}$ .

### B. Theoretical results

The CRENLB/SO basis set used in the current work has been shown previously to be suitable for Au atoms.<sup>16,57,93,94</sup> Several different functionals/basis sets were used for the S atom. The top ranked low-lying structures located for  $\text{Au}_x\text{S}^-$  ( $x = 2-5$ ) together with their relative energies and structural parameters of the corresponding isomers are depicted in Fig. 2 and Figs. S1 and S2 in the supplementary material.<sup>95</sup> The global minima of neutral  $\text{Au}_x\text{S}$  are also shown in Fig. 2.

#### 1. $\text{Au}_2\text{S}^-$ and $\text{Au}_2\text{S}$

All calculations using different methods indicate that the global minimum of  $\text{Au}_2\text{S}^-$  is an asymmetric linear species with  $C_{\infty v}$  symmetry (Fig. 2). The bent structure with  $C_{2v}$  sym-

metry is higher in energy by all the methods used in this study. The energies of the  $C_{2v}$  structure relative to the linear global minimum range from 0.61 eV to 0.98 eV at different levels of DFT calculations. The higher level *ab initio* methods (MP2) gave an even higher energy of 1.03 eV for the  $C_{2v}$  structure relative to the linear structure. At the CCSD(T) level, the bent structure is 0.74 eV higher in energy than the linear global minimum.

We employed four methods to search for the global minimum of neutral  $\text{Au}_2\text{S}$ : the pure PBE functional, the hybrid B3LYP functional, the higher level MP2 theory, and the highest CCSD(T) level of theory. All methods predict that the global minimum is the bent  $C_{2v}$  structure (Fig. 2). The  $C_{\infty v}$  linear isomer is found to be  $\sim 2$  eV higher than the bent global minimum at the MP2 level. However, the  $C_{\infty v}$  linear isomer is a true minimum, which is accessed in the detachment from the linear anion. The relatively high energy of the linear structure in the neutral potential energy surface explains why the VDE of  $\text{Au}_2\text{S}^-$  is so high. The highly stable bent neutral  $\text{Au}_2\text{S}$  ( $C_{2v}$ ) is analogous to the  $C_{2v}$   $\text{H}_2\text{S}$  molecule, demonstrating that Au mimics H in its bonding to sulfur. The Au/H analogy has been found previously in Si–Au<sup>49,96,97</sup> and B–Au<sup>54,64</sup> clusters.

#### 2. $\text{Au}_3\text{S}^-$ and $\text{Au}_3\text{S}$

We found that the global minimum of  $\text{Au}_3\text{S}^-$  is an asymmetric bent structure (Au–S–Au–Au) with  $C_s$  symmetry ( $^1A$ ), while the rhombus structure with  $C_{2v}$  symmetry is the second isomer much higher in energy (Fig. 2). We obtained similar results by higher levels of theory, such as MP2, MP4, CCSD, and CCSD(T) (Table S1).<sup>95</sup> We also studied the structures of neutral  $\text{Au}_3\text{S}$  using different methods. The most stable neutral also has  $C_s$  symmetry with a similar bent structure as the anion at the B3LYP level. However, at higher levels of theory (MP2 and CCSD(T)), we found that the global minimum of  $\text{Au}_3\text{S}$  favors the  $C_{2v}$  planar structure (Fig. 2), similar to that reported previously.<sup>73</sup>

#### 3. $\text{Au}_4\text{S}^-$ and $\text{Au}_4\text{S}$

The global minimum of  $\text{Au}_4\text{S}^-$  is found to be a bent structure with  $C_{2v}$  symmetry (Fig. 2), which is formed by adding a Au atom to the global minimum of  $\text{Au}_3\text{S}^-$ . The second higher isomer of  $\text{Au}_4\text{S}^-$  is a 2D planar structure with  $C_s$  symmetry, which is formed by adding a Au atom to the second isomer of  $\text{Au}_3\text{S}^-$ . This isomer is 0.11 eV higher than the global minimum 1D bent structure. For neutral  $\text{Au}_4\text{S}$ , we found it to favor the planar structure with  $C_s$  symmetry (Fig. 2). Because the photoelectron spectra of the main isomer of  $\text{Au}_4\text{S}^-$  display no HOMO-LUMO gap, suggesting its corresponding neutral ground state should be a triplet state, we calculated various spin multiplicities at the B3LYP level for the 1D and 2D isomers of neutral  $\text{Au}_4\text{S}$ . We found that for the planar isomer ( $C_s$ ), the singlet ( $^1A_1$ ) is the most stable electronic state, and indeed for the bent isomer ( $C_{2v}$ ) of neutral  $\text{Au}_4\text{S}$ , the triplet ( $^3A'$ ) state is the ground electronic state, more stable than the singlet state by  $\sim 0.64$  eV, consistent with the experimental observation.

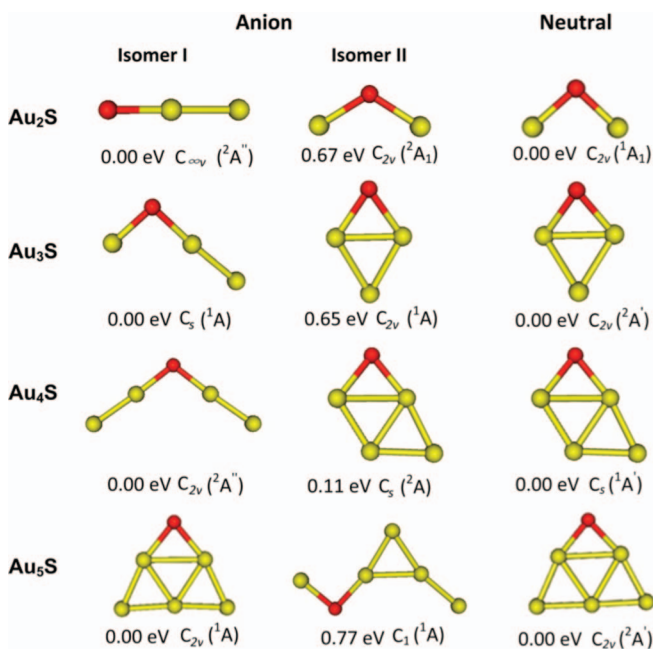


FIG. 2. Optimized structures for the global minimum and low-lying isomers of  $\text{Au}_x\text{S}^-$  ( $x = 2-5$ ) and the global minima of the neutrals. The relative energies are in eV for each structures at B3LYP/6-31++G\*\* level for the anions.

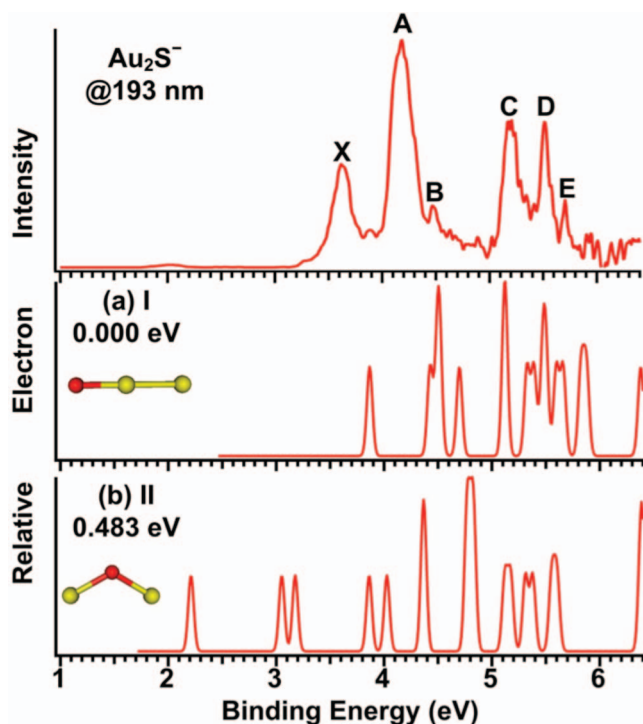


FIG. 3. Comparison of the simulated spectra for the global minimum of  $\text{Au}_2\text{S}^-$  (a) and the nearest low-lying isomer (b) with the experimental spectrum (upper panel), at the B3LYP/6-311++G(3df,3pd)//B3LYP/6-31++G\*\* level. The insets show the corresponding structures and relative energies for the two isomers.

#### 4. $\text{Au}_5\text{S}^-$ and $\text{Au}_5\text{S}$

We used several methods to calculate the low-lying structures of  $\text{Au}_5\text{S}^-$  and  $\text{Au}_5\text{S}$ . We found that all methods give the 2D triangular structure with  $C_{2v}$  symmetry as the lowest energy isomer for both the neutral and anion (Fig. 2). This structure is similar to the triangular structure of  $\text{Au}_6$ .<sup>13,15,98</sup> The second isomer is at least 0.77 eV higher in energy.

#### 5. PES spectral simulations

We simulated the PES spectra of the global minima and low-lying isomers by fitting the computed VDEs with Gaussian functions of 0.04 eV width. The simulated spectra are compared with the experimental spectra in Figs. 3–6 for  $\text{Au}_x\text{S}^-$  ( $x = 2-5$ ), respectively. More simulated spectra at different levels of theory are given in Figs. S3–S5 for  $\text{Au}_x\text{S}^-$  ( $x = 3-5$ ) in the supplementary material.<sup>95</sup>

### IV. DISCUSSION

The well-resolved PES spectra of  $\text{Au}_x\text{S}^-$  ( $x = 2-5$ ) allow a detailed comparison with theoretical simulations using different combinations of functionals/basis sets at the DFT level. Compared with the high level methods, such as CCSD, CCSD(T), or MP2/MP4, DFT methods have been more widely used, due to the less computational costs and relatively good accuracy, providing possibilities for much larger systems to be studied.<sup>33,99</sup> In order to identify the appropriate functionals and basis sets to describe and

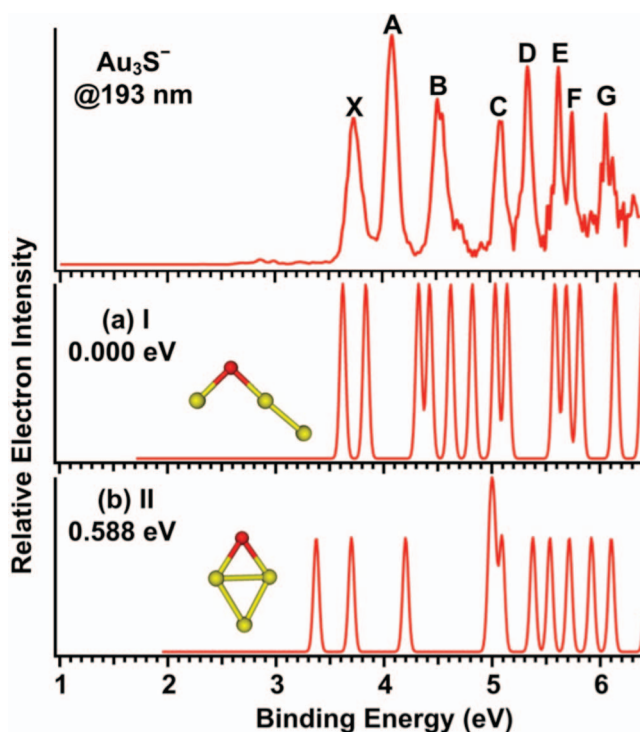


FIG. 4. Comparison of the simulated spectra for the global minimum of  $\text{Au}_3\text{S}^-$  (a) and the nearest low-lying isomer (b) with the experimental spectrum (upper panel), at the B3LYP/6-311++G(3df,3pd)//B3LYP/6-31++G\*\* level. The insets show the corresponding structures and relative energies for the two isomers.

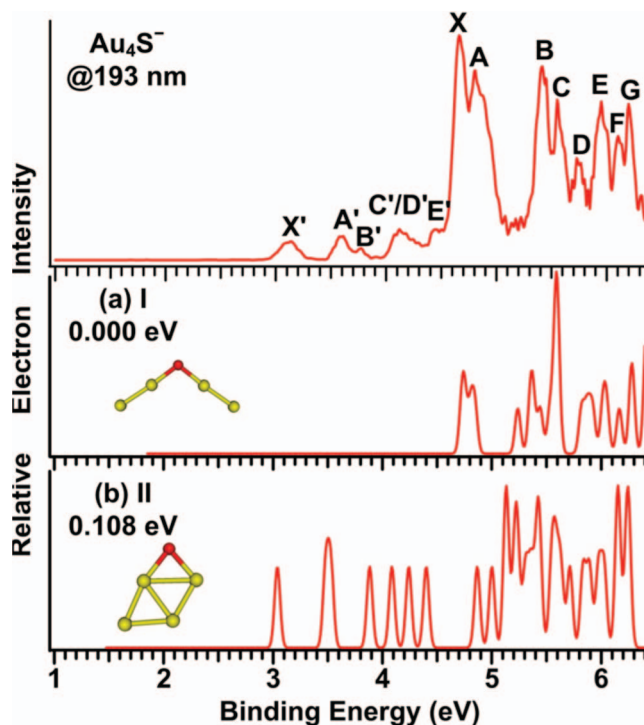


FIG. 5. Comparison of the simulated spectra for the global minimum of  $\text{Au}_4\text{S}^-$  (a) and the nearest low-lying isomer (b) with the experimental spectrum (upper panel), at the B3LYP/6-311++G(3df,3pd)//B3LYP/6-31++G\*\* level. The insets show the corresponding structures and relative energies for the two isomers.

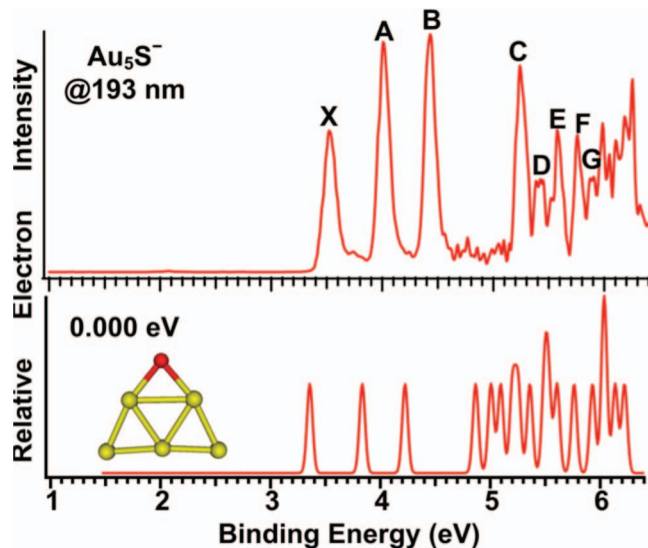


FIG. 6. Comparison of the simulated spectrum for the global minimum of  $\text{Au}_5\text{S}^-$  with the experimental spectrum (upper panel), at the B3LYP/6-311++G(3df,3pd)//B3LYP/6-31++G\*\* level.

characterize the Au–S systems, we tested different DFT methods to simulate PES spectra for comparison with the experimental results. We found that calculations at the B3LYP/6-311++G(3df,3pd)//B3LYP/6-31++G\*\* level give reasonably consistent results in comparison to the experimental data (Figs. 3–6).

## A. Comparison of the theoretical and experimental results

### 1. $\text{Au}_2\text{S}^-$

The simulated spectra of the global minimum and the second isomer of  $\text{Au}_2\text{S}^-$  are compared with the 193 nm PES spectrum in Fig. 3. The simulated spectral pattern from the global minimum linear structure ( $C_{\infty v}$ ) is found to agree well with the experimental data. The first calculated VDE and the VDEs corresponding to bands A and B are slightly overestimated, which is in line with previous studies.<sup>57,63,94</sup> The VDEs of the second and third detachment channels are closely spaced, consistent with the observed band A, which seems to contain multiple electronic transitions. There are more detachment transitions in the higher binding energy range, which are not well resolved in the experimental spectrum. On the other hand, the bent  $C_{2v}$  isomer gives rise to very low VDEs and yields a spectral pattern, which disagrees with the experimental spectrum.

### 2. $\text{Au}_3\text{S}^-$

The simulated PES spectra at the B3LYP level for the global minimum 1D bent structure and the low-lying rhombus 2D planar isomer of  $\text{Au}_3\text{S}^-$  are compared with the experimental data in Fig. 4. More simulated spectra at PBE0 levels are given in Fig. S3.<sup>95</sup> The calculated first VDE of the 1D global minimum is 3.61 eV, in very good agreement with the experimental VDE of 3.72 eV. At the PBE0 levels, the calcu-

lated first VDE for the bent global minimum is also in good agreement with the experiment. On the other hand, the first VDE calculated for the 2D planar isomer at all levels of theory is much lower than the experimental VDE. However, the spectral pattern simulated from the 1D global minimum does not seem to be in good agreement with the experiment. Even though the first three bands in the simulated spectrum for the 2D planar isomer appear to be consistent with the experiment, the gap between the third and fourth detachment bands is too large in comparison with the experiment.

The relative energy of the 2D isomer is higher than the 1D global minimum by 0.65 eV at the B3LYP level, suggesting that the 2D isomer is unlikely to be populated in the cluster beam. We further carried out higher level *ab initio* calculations, including geometry optimizations at the MP2, MP4, CCSD, and CCSD(T) levels with the Au/aug-cc-pvdz-pp/S/6-31+G\* basis set. All the higher level *ab initio* calculations gave similar results as the DFT methods (Table S1).<sup>95</sup> Thus, we conclude that the 1D structure is the global minimum for  $\text{Au}_3\text{S}^-$ .

### 3. $\text{Au}_4\text{S}^-$

The simulated PES spectra of the global minimum 1D bent structure and the low-lying 2D planar isomer for  $\text{Au}_4\text{S}^-$  are compared with the 193 nm experimental spectrum in Fig. 5. The global minimum bent structure gives much higher VDEs and its simulated spectrum is in good agreement with the main features observed experimentally. On the other hand, the VDEs calculated for the low-lying planar isomer are much lower and its simulated spectrum agrees well with the weaker low binding energy features observed experimentally. Higher binding energy detachment features from the 2D isomer overlap with the detachment features from the main bent isomer. We also simulated the PES spectra of the two isomers at several other levels of theory (Fig. S4)<sup>95</sup> and they all agree qualitatively with the experimental data. Hence, there is no question that the 2D planar isomer was present in the cluster beam, consistent with that fact that this isomer is close in energy to the global minimum bent isomer, only 0.11 eV higher at the B3LYP level. In reality, the relative energy of the 2D isomer is likely to be even closer to the bent structure, because our cluster beam is quite cold.<sup>100</sup>

### 4. $\text{Au}_5\text{S}^-$

The simulated spectrum of the global minimum planar structure for  $\text{Au}_5\text{S}^-$  at the B3LYP level is compared with the 193 nm experimental data in Fig. 6. Both the calculated first VDE and the simulated spectral pattern are in good agreement with the experimental data. We also simulated the spectrum of  $\text{Au}_5\text{S}^-$  at several PBE levels (Fig. S5)<sup>95</sup> and they are all in good agreement with the experimental spectrum, unequivocally confirming the planar global minimum structure for  $\text{Au}_5\text{S}^-$ . The structure of  $\text{Au}_5\text{S}^-$  is similar to the triangular structures of  $\text{Au}_6$  and  $\text{Au}_6^-$ ,<sup>13,15,98</sup> with the sulfur atom replacing one apex Au atom.

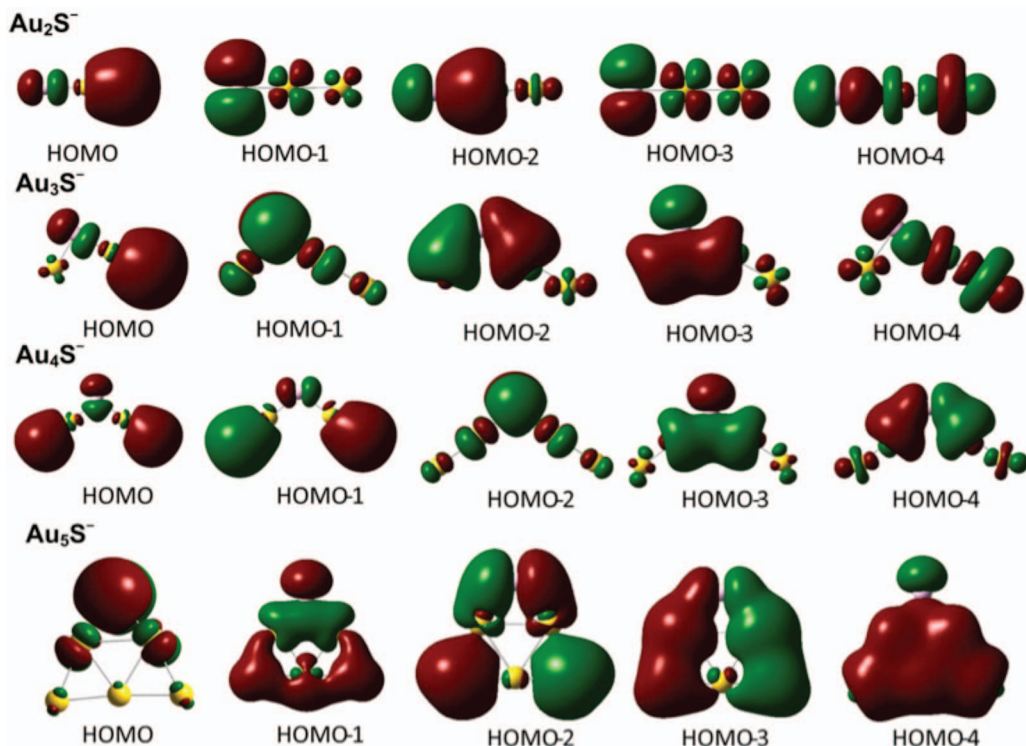


FIG. 7. The top molecular orbital pictures for the global minima of  $Au_x S^-$  ( $x = 2-5$ ).

## B. Structural and chemical bonding evolution

A 1D to 2D structural transition in the  $Au_x S^-$  ( $x = 2-5$ ) series of S doped gold clusters is observed. For  $x = 2-4$ , the 1D structures are more stable, whereas at  $x = 5$  the 2D structure is more favored. The transition occurs at  $x = 4$ , for which the 2D planar structure becomes competitive and coexist with the 1D bent global minimum experimentally. The structural change reflects the underlying chemical bonding. The stable 1D structure is a result of the strong S–Au covalent bonds, as shown previously for  $AuS^-$  and  $Au_2S^-$ .<sup>63,72</sup> As the number of gold atoms increases, the Au–Au interaction becomes important and the 2D planar structures gain stability. The top few valence molecular orbitals for the global minima of  $Au_x S^-$  ( $x = 2-5$ ) are shown in Fig. 7. One can see the localized MOs due to S–Au bonding for the 1D clusters from  $x = 2-4$  and the multi-center delocalized Au–Au bonding in the  $Au_5S^-$  cluster. The strong Au–S covalent bonding dominates the structures of  $Au_x S^-$  ( $x = 2-4$ ), resulting in the 1D type structures.

The EA trend is also very interesting: the 1D clusters have much large EAs than the 2D clusters. This is shown more dramatically by the large EA difference of the two isomers of  $Au_4S$ . The EA represents electron detachment from the HOMO of each cluster. The MO pictures shown in Fig. 7 provide a nice explanation of the EA trend between the 1D and 2D clusters. The HOMOs of the three 1D clusters are all mainly of Au 6s characters, which are highly stabilized due to the relativistic effects as also reflected in the unusually high EA of the Au atom. On the other hand, the HOMO of the 2D  $Au_5S^-$  cluster is mainly localized on the S atom, which has a lower EA than that of the Au atom. The extremely high EA of

the 1D structure of  $Au_4S$  is also due to the fact that it has an open-shell triplet ground electronic state.

## V. CONCLUSIONS

In conclusion, we report an investigation of the structures and bonding of a series of sulfur-doped gold clusters,  $Au_x S^-$  ( $x = 2-5$ ), using photoelectron spectroscopy and theoretical calculations at several levels of theory. A hybrid DFT method is found to give satisfactory results in comparison with the experimental data.  $Au_2S^-$  is found to have an asymmetric linear structure (S–Au–Au), while neutral  $Au_2S$  possesses a bent  $C_{2v}$  structure similar to  $H_2S$ .  $Au_3S^-$  has an interesting asymmetric bent structure with a Au–S–Au–Au connectivity. For  $Au_4S^-$ , both a symmetric bent structure (Au–Au–S–Au–Au) and a planar structure are found to be close in energy and coexist experimentally.  $Au_5S^-$  is found to possess a triangular planar structure. Thus, a 1D to 2D transition is observed at  $Au_4S^-$ . The 1D structures are due to the strong S–Au covalent bonding. As the number of gold atoms increases, Au–Au delocalized bonding becomes important, favoring the 2D planar structures.

## ACKNOWLEDGMENTS

The experimental work was supported by the National Science Foundation (Grant No. CHE-1049717 to L.S.W.). The theoretical work was supported by grants from the National Natural Science Foundation of China (Grant Nos. 21073196 and 21133008), Director Fund of AIOFM, CAS.

- <sup>1</sup>P. Pyykkö, *Angew. Chem., Int. Ed.* **43**, 4412 (2004).
- <sup>2</sup>P. Pyykkö, *Inorg. Chim. Acta* **358**, 4113 (2005).
- <sup>3</sup>M. Haruta, *Catal. Today* **36**, 153 (1997).
- <sup>4</sup>G. J. Hutchings, M. Brust, and H. Schmidbaur, *Chem. Soc. Rev.* **37**(9), 1759 (2008) [Special issue: Gold – Chemistry, Materials and Catalysis].
- <sup>5</sup>J. Ho, K. M. Ervin, and W. C. Lineberger, *J. Chem. Phys.* **93**, 6987 (1990).
- <sup>6</sup>K. J. Taylor, C. Jin, J. Conceicao, L. S. Wang, O. Cheshnovsky, B. R. Johnson, P. J. Nordlander, and R. E. Smalley, *J. Chem. Phys.* **93**, 7515 (1990).
- <sup>7</sup>K. J. Taylor, C. L. Pettiettehall, O. Cheshnovsky, and R. E. Smalley, *J. Chem. Phys.* **96**, 3319 (1992).
- <sup>8</sup>H. Handschuh, G. Gantefor, P. S. Bechthold, and W. Eberhardt, *J. Chem. Phys.* **100**, 7093 (1994).
- <sup>9</sup>H. Schmidbaur, *Chem. Soc. Rev.* **24**, 391 (1995).
- <sup>10</sup>I. L. Garzon, K. Michaelian, M. R. Beltran, A. Posada-Amarillas, P. Ordejon, E. Artacho, D. Sanchez-Portal, and J. M. Soler, *Phys. Rev. Lett.* **81**, 1600 (1998).
- <sup>11</sup>H. Schmidbaur, *Nature (London)* **413**, 31 (2001).
- <sup>12</sup>F. Furche, R. Ahlrichs, P. Weis, C. Jacob, S. Gilb, T. Bierweiler, and M. M. Kappes, *J. Chem. Phys.* **117**, 6982 (2002).
- <sup>13</sup>S. Gilb, P. Weis, F. Furche, R. Ahlrichs, and M. M. Kappes, *J. Chem. Phys.* **116**, 4094 (2002).
- <sup>14</sup>H. Hakkinen, M. Moseler, and U. Landman, *Phys. Rev. Lett.* **89**, 033401 (2002).
- <sup>15</sup>H. Hakkinen, B. Yoon, U. Landman, X. Li, H. J. Zhai, and L. S. Wang, *J. Phys. Chem. A* **107**, 6168 (2003).
- <sup>16</sup>J. Li, X. Li, H.-J. Zhai, and L.-S. Wang, *Science* **299**, 864 (2003).
- <sup>17</sup>S. Gilb, K. Jacobsen, D. Schooss, F. Furche, R. Ahlrichs, and M. M. Kappes, *J. Chem. Phys.* **121**, 4619 (2004).
- <sup>18</sup>H. Hakkinen, M. Moseler, O. Kostko, N. Morgner, M. A. Hoffmann, and B. v. Issendorff, *Phys. Rev. Lett.* **93**, 093401 (2004).
- <sup>19</sup>S. Bulusu, X. Li, L. S. Wang, and X. C. Zeng, *Proc. Natl. Acad. Sci. U.S.A.* **103**, 8326 (2006).
- <sup>20</sup>S. Bulusu and X. C. Zeng, *J. Chem. Phys.* **125**, 154305 (2006).
- <sup>21</sup>X. P. Xing, Y. Bokwon, U. Landman, and J. H. Parks, *Phys. Rev. B* **74**, 165423 (2006).
- <sup>22</sup>A. Lechtken, D. Schooss, J. R. Stairs, M. N. Blom, F. Furche, N. Morgner, O. Kostko, B. v. Issendorff, and M. M. Kappes, *Angew. Chem., Int. Ed.* **46**, 2944 (2007).
- <sup>23</sup>X. Li, S. Bulusu, L. S. Wang, and X. C. Zeng, *J. Phys. Chem. C* **111**, 4190 (2007).
- <sup>24</sup>S. Bulusu, X. Gu, X. Li, X. C. Zeng, Jun Li, X. G. Gong, and L. S. Wang, *J. Phys. Chem. C* **111**, 8228 (2007).
- <sup>25</sup>H. Hakkinen, *Chem. Soc. Rev.* **37**, 1847 (2008).
- <sup>26</sup>M. P. Johansson, A. Lechtken, D. Schooss, M. M. Kappes, and F. Furche, *Phys. Rev. A* **77**, 053202 (2008).
- <sup>27</sup>W. Huang, M. Ji, C. D. Dong, X. Gu, L. M. Wang, X. G. Gong, and L. S. Wang, *ACS Nano* **2**, 897 (2008).
- <sup>28</sup>L. Ferrighi, B. Hammer, and G. K. H. Madsen, *J. Am. Chem. Soc.* **131**, 10605 (2009).
- <sup>29</sup>W. Huang and L. S. Wang, *Phys. Chem. Chem. Phys.* **11**, 2663 (2009).
- <sup>30</sup>A. Lechtken, C. Neiss, M. M. Kappes, and D. Schooss, *Phys. Chem. Chem. Phys.* **11**, 4344 (2009).
- <sup>31</sup>M. Mantina, R. Valero, and D. G. Truhlar, *J. Chem. Phys.* **131**, 064706 (2009).
- <sup>32</sup>A. Yang, W. Fa, and J. Dong, *Phys. Lett. A* **374**, 4506 (2010).
- <sup>33</sup>W. Huang, N. Shao, Y. Gao, L. M. Wang, X. Li, L. S. Wang, and X. C. Zeng, *J. Am. Chem. Soc.* **132**, 6596 (2010).
- <sup>34</sup>A. Roldan, J. M. Ricart, F. Illas, and G. Pacchioni, *Phys. Chem. Chem. Phys.* **12**, 10723 (2010).
- <sup>35</sup>D. Schooss, P. Weis, O. Hampe, and M. M. Kappes, *Philos. Trans. R. Soc. London, Ser. A* **368**, 1211 (2010).
- <sup>36</sup>R. W. Burgess and V. J. Keast, *J. Phys. Chem. C* **115**, 21016 (2011).
- <sup>37</sup>H. S. De, S. Krishnamurty, D. Mishra, and S. Pal, *J. Phys. Chem. C* **115**, 17278 (2011).
- <sup>38</sup>D. E. Jiang and M. Walter, *Phys. Rev. B* **84**, 193402 (2011).
- <sup>39</sup>Y. Dong, M. Springborg, and I. Warnke, *Theor. Chem. Acc.* **130**, 1001 (2011).
- <sup>40</sup>D. X. Tian, J. Li, Y. Zhao, J. J. Zhao, and X. Y. Guo, *Comput. Mater. Sci.* **50**, 2359 (2011).
- <sup>41</sup>R. Pal, L. M. Wang, W. Huang, L. S. Wang, and X. C. Zeng, *J. Chem. Phys.* **134**, 054306 (2011).
- <sup>42</sup>C. Briones-Jurado, P. de la Mora, and E. Agacino-Valdes, *Int. J. Quantum Chem.* **112**, 3646 (2012).
- <sup>43</sup>J. V. Koppen, M. Hapka, M. M. Szczesniak, and G. Chalasiński, *J. Chem. Phys.* **137**, 114302 (2012).
- <sup>44</sup>R. Lei and C. Longjiu, *Comput. Theor. Chem.* **984**, 142 (2012).
- <sup>45</sup>L. M. Wang and L. S. Wang, *Nanoscale* **4**, 4038 (2012).
- <sup>46</sup>B. Pauwels, G. V. Tendeloo, E. Zhurkin, M. Hou, G. Verschoren, L. T. Kuhn, W. Bouwen, and P. Lievens, *Phys. Rev. B* **63**, 165406 (2001).
- <sup>47</sup>S. Neukermans, E. Janssens, H. Tanaka, R. E. Silverans, and P. Lievens, *Phys. Rev. Lett.* **90**, 033401 (2003).
- <sup>48</sup>H. Tanaka, S. Neukermans, E. Janssens, R. E. Silverans, and P. Lievens, *J. Chem. Phys.* **119**, 7115 (2003).
- <sup>49</sup>X. Li, B. Kiran, H. J. Zhai, L. F. Cui, and L. S. Wang, *Angew. Chem., Int. Ed.* **43**, 2125 (2004).
- <sup>50</sup>H. J. Zhai, J. Li, and L. S. Wang, *J. Chem. Phys.* **121**, 8369 (2004).
- <sup>51</sup>H. J. Zhai, B. Kiran, and L. S. Wang, *J. Chem. Phys.* **121**, 8231 (2004).
- <sup>52</sup>X. Li, B. Kiran, L. F. Cui, and L. S. Wang, *Phys. Rev. Lett.* **95**, 253401 (2005).
- <sup>53</sup>Y. Gao, S. Bulusu, and X. C. Zeng, *Chem. Phys. Chem.* **7**, 2275 (2006).
- <sup>54</sup>H. J. Zhai, L. S. Wang, D. Y. Zubarev, and A. I. Boldyrev, *J. Phys. Chem. A* **110**, 1689 (2006).
- <sup>55</sup>H. W. Ghebriel and A. Kshirsagar, *J. Chem. Phys.* **126**, 244705 (2007).
- <sup>56</sup>N. Veldeman, E. Janssens, K. Hansen, J. De Haecck, R. E. Silverans, and P. Lievens, *Faraday Discuss.* **138**, 147 (2008).
- <sup>57</sup>L. M. Wang, R. Pal, W. Huang, X. C. Zeng, and L. S. Wang, *J. Chem. Phys.* **130**, 051101 (2009).
- <sup>58</sup>L.-M. Wang, J. Bai, A. Lechtken, W. Huang, D. Schooss, M. M. Kappes, X. C. Zeng, and L. S. Wang, *Phys. Rev. B* **79**, 033413 (2009).
- <sup>59</sup>L. M. Wang, R. Pal, W. Huang, X. C. Zeng, and L. S. Wang, *J. Chem. Phys.* **132**, 114306 (2010).
- <sup>60</sup>L. Ling, P. Claes, T. Holtz, E. Janssens, T. Wende, R. Bergmann, G. Santambrogio, G. Meijer, K. R. Asmis, N. M. Tho, and P. Lievens, *Phys. Chem. Chem. Phys.* **12**, 13907 (2010).
- <sup>61</sup>S. Nigam and C. Majumder, *J. Phys.: Condens. Matter* **22**, 435001 (2010).
- <sup>62</sup>A. H. Pakiari and Z. Jamshidi, *J. Phys. Chem. A* **114**, 9212 (2010).
- <sup>63</sup>L. S. Wang, *Phys. Chem. Chem. Phys.* **12**, 8694 (2010).
- <sup>64</sup>H. J. Zhai, C. Q. Miao, S. D. Li, and L. S. Wang, *J. Phys. Chem. A* **114**, 12155 (2010).
- <sup>65</sup>J. d. Haecck, N. Veldeman, P. Claes, E. Janssens, M. Andersson, and P. Lievens, *J. Phys. Chem. A* **115**, 2103 (2011).
- <sup>66</sup>D. Die, X. Y. Kuang, B. Zhu, and J. J. Guo, *Physica B* **406**, 3160 (2011).
- <sup>67</sup>G. X. Ge, H. X. Yan, Q. Jing, and J. J. Zhang, *Acta Phys. Sin.* **60**, 033101 (2011).
- <sup>68</sup>J. X. Yi, J. J. Guo, and D. Dong, *Comput. Theor. Chem.* **963**, 435 (2011).
- <sup>69</sup>X. Y. Li, *J. Mol. Model.* **18**, 1003 (2012).
- <sup>70</sup>Y. Li, Y. P. Cao, Y. F. Li, S. P. Shi, and X. Y. Kuang, *Eur. Phys. J. D* **66**, 10 (2012).
- <sup>71</sup>F. Rabilloud, *J. Phys. Chem. A* **116**, 3474 (2012).
- <sup>72</sup>H. J. Zhai, C. Burgel, V. Bonacic-Koutecky, and L. S. Wang, *J. Am. Chem. Soc.* **130**, 7244 (2008).
- <sup>73</sup>C. Majumder and S. K. Kulshreshtha, *Phys. Rev. B* **73**, 155427 (2006).
- <sup>74</sup>G. Bravo-Perez and I. L. Garzon, *J. Mol. Struct.* **619**, 79 (2002).
- <sup>75</sup>J. M. Seminario, C. E. de la Cruz, and P. A. Derosa, *J. Am. Chem. Soc.* **123**, 5616 (2001).
- <sup>76</sup>X. Wang, B. Liang, and L. Andrews, *Dalton Trans.* **2009**, 4190.
- <sup>77</sup>T. Rietmann, S. Sohn, M. Schröder, D. Lipinsky, and H. F. Arlinghaus, *Appl. Surf. Sci.* **252**, 6640 (2006).
- <sup>78</sup>T. Ichino, A. J. Gianola, D. H. Andrews, and W. C. Lineberger, *J. Phys. Chem. A* **108**, 11307 (2004).
- <sup>79</sup>W. J. Huang, Z. Y. Liu, R. B. Huang, and L. S. Zheng, *Acta Chim. Sin.* **56**, 200 (1998).
- <sup>80</sup>C. G. Ning, X. G. Xiong, Y. L. Wang, J. Li, and L. S. Wang, *Phys. Chem. Chem. Phys.* **14**, 9323 (2012).
- <sup>81</sup>Y. Pei, N. Shao, H. Li, D. E. Jiang, and X. C. Zeng, *ACS Nano* **5**, 1441 (2011).
- <sup>82</sup>M. Zhang, S. Chen, Q. M. Deng, L. M. He, L. N. Zhao, and Y. H. Luo, *Eur. Phys. J. D* **58**, 117 (2010).
- <sup>83</sup>D. E. Jiang, M. Walter, and S. Dai, *Chem. Eur. J.* **16**, 4999 (2010).
- <sup>84</sup>H. Woldegebrhel and A. Kshirsagar, *J. Chem. Phys.* **127**, 224708 (2007); A. A. Bagatur'yants, A. A. Safonov, H. Stoll, and H. J. Werner, *ibid.* **109**, 3096 (1998); K. Sugawara, F. Sobott, and A. B. Vakhtin, *ibid.* **118**, 7808 (2003).
- <sup>85</sup>C. Majumder, A. K. Kandalam, and P. Jena, *Phys. Rev. B* **74**, 205437 (2006).
- <sup>86</sup>P. Pyykkö, K. Angermaier, B. Assmann, and H. Schmidbaur, *J. Chem. Soc. Chem. Commun.* **1995**, 1889.

- <sup>87</sup>L. S. Wang, H. S. Cheng, and J. Fan, *J. Chem. Phys.* **102**, 9480 (1995).
- <sup>88</sup>L. S. Wang and H. Wu, in *Advances in Metal and Semiconductor Clusters. IV. Cluster Materials*, edited by M. A. Duncan (JAI Press, Greenwich, 1998), pp. 299–343.
- <sup>89</sup>H. J. Zhai, W. Huang, and L. S. Wang, *J. Am. Chem. Soc.* **132**, 4344 (2010).
- <sup>90</sup>J. Akola, M. Manninen, H. Hakkinen, U. Landman, X. Li, and L.-S. Wang, *Phys. Rev. B* **60**, R11297 (1999).
- <sup>91</sup>Y. L. Wang, H. J. Zhai, X. Lu, J. Li, and L. S. Wang, *J. Phys. Chem. A* **114**, 1247 (2010).
- <sup>92</sup>E. L. Bylaska *et al.*, NWChem, a computational chemistry package for parallel computers, version 5.1.1, Pacific Northwest National Laboratory, Richland, USA.
- <sup>93</sup>X. Li, B. Kiran, J. Li, H. J. Zhai, and L. S. Wang, *Angew. Chem., Int. Ed.* **41**, 4786 (2002).
- <sup>94</sup>W. Huang, R. Pal, L. M. Wang, X. C. Zeng, and L. S. Wang, *J. Chem. Phys.* **132**, 054305 (2010).
- <sup>95</sup>See supplementary material at <http://dx.doi.org/10.1063/1.4802477> for more information on relative energies, structures, and simulated PES spectra of low-lying isomers of each cluster.
- <sup>96</sup>X. Li, B. Kiran, and L. S. Wang, *J. Phys. Chem. A* **109**, 4366 (2005).
- <sup>97</sup>B. Kiran, X. Li, H. J. Zhai, and L. S. Wang, *J. Chem. Phys.* **125**, 133204 (2006).
- <sup>98</sup>H. J. Zhai, B. Kiran, B. Dai, J. Li, and L. S. Wang, *J. Am. Chem. Soc.* **127**, 12098 (2005).
- <sup>99</sup>P. Geerlings, F. De Proft, and W. Langenaeker, *Chem. Rev.* **103**, 1793 (2003).
- <sup>100</sup>W. Huang and L. S. Wang, *Phys. Rev. Lett.* **102**, 153401 (2009).